Thin-film composite forward osmosis membranes functionalized with graphene oxide-silver nanocomposites for biofouling control

Andreia Faria
Yale University

Caihong Liu
Yale University, Harbin Institute of Technology

Ming Xie
Yale University, Victoria University, mx504@uowmail.edu.au

Francois Perreault
Yale University, Arizona State University

Long D. Nghiem
University of Wollongong, longn@uow.edu.au

See next page for additional authors

Recommended Citation

Thin-film composite forward osmosis membranes functionalized with graphene oxide-silver nanocomposites for biofouling control

Abstract

Innovative approaches to prevent bacterial attachment and biofilm growth on membranes are critically needed to avoid decreasing membrane performance due to biofouling. In this study, we propose the fabrication of anti-biofouling thin-film composite membranes functionalized with graphene oxide-silver nanocomposites. In our membrane modification strategy, carboxyl groups on the graphene oxide-silver nanosheets are covalently bonded to carboxyl groups on the surface of thin-film composite membranes via a crosslinking reaction. Further characterization, such as scanning electron microscopy and Raman spectroscopy, revealed the immobilization of graphene oxide-silver nanocomposites on the membrane surface. Graphene oxide-silver modified membranes exhibited an 80% inactivation rate against attached . *Pseudomonas aeruginosa* cells. In addition to a static antimicrobial assay, our study also provided insights on the anti-biofouling property of forward osmosis membranes during dynamic operation in a cross-flow test cell. Functionalization with graphene oxide-silver nanocomposites resulted in a promising anti-biofouling property without sacrificing the membrane intrinsic transport properties. Our results demonstrated that the use of graphene oxide-silver nanocomposites is a feasible and attractive approach for the development of anti-biofouling thin-film composite membranes.

Disciplines

Engineering | Science and Technology Studies

Publication Details

Authors

Andreia Faria, Caihong Liu, Ming Xie, Francois Perreault, Long D. Nghiem, Jun Ma, and Menachem Elimelech

Thin-film composite forward osmosis membranes functionalized with graphene oxide–silver nanocomposites for biofouling control

Andreia F. Faria[1], Caihong Liu[1,2], Ming Xie[1,3], Francois Perreault[1,4], Long D. Nghiem[5], Jun Ma[2], and Menachem Elimelech[1*]

[1]*Department of Chemical and Environmental Engineering, Yale University, New Haven, Connecticut 06520-8286, USA*

[2] *State Key Laboratory of Urban Water Resource and Environment, Harbin Institute of Technology, Harbin 150090, China*

[3]*Institute for Sustainability and Innovation, College of Engineering and Science, Victoria University, PO Box 14428, Melbourne, Victoria 8001, Australia*

[4]*School of Sustainable Engineering and the Built Environment, Arizona State University, Tempe, AZ, 85287-3005.*

[5] *Water Infrastructure Laboratory, School of Civil, Mining and Environmental Engineering, University of Wollongong, Wollongong, NSW 2522, Australia*

* Corresponding author: Menachem Elimelech, Email: menachem.elimelech@yale.edu, Phone: (203) 432-2789

ABSTRACT

Innovative approaches to prevent bacterial attachment and biofilm growth on membranes are critically needed to avoid decreasing membrane performance due to biofouling. In this study, we propose the fabrication of anti-biofouling thin-film composite membranes functionalized with graphene oxide−silver nanocomposites. In our membrane modification strategy, carboxyl groups on the graphene oxide−silver nanosheets are covalently bonded to carboxyl groups on the surface of thin-film composite membranes via a crosslinking reaction. Further characterization, such as scanning electron microscopy and Raman spectroscopy, revealed the immobilization of graphene oxide−silver nanocomposites on the membrane surface. Graphene oxide−silver modified membranes exhibited an 80% inactivation rate against attached *Pseudomonas aeruginosa* cells. In addition to a static antimicrobial assay, our study also provides insights on the anti-biofouling property of forward osmosis membranes during dynamic operation in a cross-flow test cell. Functionalization with graphene oxide−silver nanocomposites resulted in a promising anti-biofouling property without sacrificing the membrane intrinsic transport properties. Our results demonstrated that the use of graphene oxide−silver nanocomposites is a feasible and attractive approach for the development of anti-biofouling thin-film composite membranes.

Keywords: forward osmosis, thin-film composite membranes, graphene oxide, silver nanoparticles, antimicrobial activity, biofouling control.

1. Introduction

Global demand for drinking water is expected to increase in the coming decades due to rapid population growth and climate change [1]. Membrane-based water purification processes play a crucial role in mitigating water scarcity worldwide [1, 2]. Due to their high permeate water flux and salt rejection capabilities, thin-film composite (TFC) membranes have been considered the state-of-the art for water desalination technologies such as reverse osmosis (RO) and forward osmosis (FO) [1-4]. Despite these advantages, TFC membranes encounter several operational limitations. One significant challenge is the attachment of microorganisms and subsequent biofilm formation [5, 6].

The growth of bacteria as biofilms can affect membrane performance by decreasing permeate water flux and salt rejection [6]. Furthermore, biofouling development can lead to an increase in energy consumption [5-7]. Ordinary procedures such as pretreatment and chemical cleaning are being used to mitigate biofouling [5, 6]. However, no pre-treatment can completely eliminate biofouling, and it is well known that the polyamide layer of TFC membranes undergoes degradation in the presence of chemical oxidants such as chlorine [8]. Therefore, there is a critical need to develop innovative strategies to control microbial proliferation at the membrane surface.

Several studies have proposed to modify the surface of TFC membranes with polymers [9], bio-active molecules [10], or antimicrobial nanomaterials [11] in order to impart antimicrobial activity and biofouling resistance to the membrane. For instance, it has been shown that TFC membranes functionalized with silver or copper nanoparticles presented a diminished susceptibility to biofouling [12, 13]. Alternatively, carbon-based nanomaterials such as carbon nanotubes (CNTs) and graphene oxide (GO) have also been linked to the polyamide layer to generate TFC membranes with enhanced antimicrobial properties [14-16].

Antimicrobial nanomaterials can be incorporated by embedding them within the membrane polymeric matrix [17]. Post-fabrication modification, on the other hand, is focused on the immobilization of nanomaterials at the membrane surface via physical interactions [13], chemical binding [16], or layer-by-layer techniques [18]. Because the nanomaterials are placed specifically at the membrane surface, post-fabrication functionalization is unlikely to affect significantly the properties of the polyamide layer [15, 16]. This technique is also material-and cost-efficient since fewer nanomaterials are required to tailor the membrane surface chemistry [15, 16].

85   Since the first discovery of the electronic properties of pristine graphene sheets [19],
86 researchers have joined efforts to unveil the properties and potential applications of graphene-
87 related materials. Graphene oxide, produced from the chemical exfoliation of graphite,
88 comprises a layer one atom-thick of graphene functionalized with oxygen atoms [20]. The
89 vast majority of GO applications have been driven by their scalable and low cost production,
90 high stability in water, large surface area, and abundance of oxygen-containing functional
91 groups [21, 22].

92   Owing to these chemical functionalities, GO can be easily combined with a wide
93 variety of polymers and nanoparticles. Using the GO surface to anchor silver nanoparticles
94 appears promising, especially due to the surface functional groups that serve as nucleation
95 points for particle growth [23, 24]. As the formation of silver nanoparticles (AgNPs) occurs
96 in a one-pot in-situ reaction, GO sheets work as a high surface area template for particle
97 attachment and the use of a capping agent is not required. In addition to the presence of
98 AgNPs themselves, graphene oxide−silver nanocomposites (GOAg) offer a diverse and
99 inherent presence of oxygen-containing functional groups (e.g., ketones, hydroxyl, carbonyl,
100 and carboxyl) that are important to bind graphene sheets to the surface of a wide range of
101 materials [25]. For antimicrobial purposes, GOAg sheets can simultaneously inactivate
102 bacterial cells through release of silver ions while providing a large surface area for contact
103 with microbial cells [23, 25]. These properties are highly relevant in fabricating antimicrobial
104 surfaces through chemical modification of polymeric materials with nanomaterials.

105   In this study, we demonstrate, for the first time, an innovative approach to modify TFC
106 membranes with GOAg nanocomposites and the associated effects on mitigating biofouling.
107 In addition to conventional antibacterial properties, we offer a step toward understanding how
108 biofilm formation on TFC membranes is influenced by the presence of GOAg
109 nanocomposites. Chemical modification with GOAg sheets led to a strong antimicrobial
110 activity and the resulting TFC-GOAg membranes efficiently suppressed biofilm formation
111 under cross-flow test conditions. Our results demonstrate that GO-based nanocomposites can
112 serve as building blocks to fabricate membranes with advanced properties for water
113 separation processes.

114

115 **2. Materials and Methods**

116 *2.1 Materials and Chemicals*

117   Graphite powder SP-1 was obtained from Bay Carbon (Bay City, MI, USA). Sulfuric

118   acid (H$_2$SO$_4$, 95.0%), hydrogen peroxide (H$_2$O$_2$, 30.0%), sodium chloride (NaCl crystals),

119   and sucrose were purchased from J. T. Baker (Phillipsburg, NJ, USA). Potassium persulfate

120   (K$_2$S$_2$O$_8$, 99.0%), phosphorous pentoxide (P$_2$O$_5$, 98.0%), potassium permanganate (KMnO$_4$,

121   99.0%), hydrochloric acid (HCl, 37.0%), silver nitrate (AgNO$_3$, 99%), dextrose (C$_6$H$_{12}$O$_6$,

122   99%), ammonium hydroxide (NH$_4$OH, 30%), ammonium chloride (NH$_4$Cl, 99%), potassium

123   phosphate monobasic (KH$_2$PO$_4$, 99%), calcium chloride hydrate (CaCl$_2$.H$_2$O, 99%), sodium

124   bicarbonate (NaHCO$_3$, 99%), magnesium sulfate heptahydrate (MgSO$_4$.7H$_2$O, 98%), MES

125   monohydrate (99%), HEPES buffer (99%), 1-ethyl-3-(3-dimethylaminopropyl) carbodiimide

126   hydrochloride (EDC, 98%), N-hydroxysuccinimide (NHS, 98%), ethanol (anhydrous,

127   99,5%), 3-[(3-cholamidopropyl)-dimethylammonio]-1-propane sulfonate (CHAPS, 98%),

128   dithiothreitol (DTT, 98%), and paraformaldehyde (95%) were purchased from Sigma-Aldrich

129   (St. Louis, Missouri, USA). Trichloro-1, 2, 2-trifluoroethane (Freon, 99%) was purchased

130   from America Refrigerants (Sarasota, FL, USA). Luria-broth medium for bacteria cultivation

131   was purchased from Becton, Dickinson and Company (Sparks, MD, USA). Glutaraldehyde

132   solution (50%) was acquired from Amresco (Solon, OH, USA). Sodium cacodylate buffer

133   (pH 7.4) was acquired from Electron Microscopy Sciences (Hatfield, PA, USA). Polyamide

134   thin-film composite (TFC) forward osmosis membranes were obtained from HTI (Hydration

135   Technology Innovation) (Albany, OR, USA) and stored in deionized (DI) water at 4°C prior

136   to use. DI water was supplied by a Millipore System (Millipore Co., Billerica, MA, USA).

137   *2.2 Graphene oxide and graphene oxide–silver (GOAg) synthesis*

138   GO was synthesized using a modified Hummers and Offemans' method [26], and its

139   details have been provided in previous publications [25, 27, 28]. Succinctly, a graphite

140   sample was subjected to two consecutive oxidation processes. First, graphite powder (1.0 g)

141   was placed in H$_2$SO$_4$ (5 mL) and pre-oxidized in the presence of K$_2$S$_2$O$_8$ (1.0 g) and P$_2$O$_5$ (1.0

142   g) at 80°C for 4.5 hours. Then, the resulting black solid (pre-oxidized) was placed into H$_2$SO$_4$

143   (40 mL) and reacted with KMnO$_4$ (5.0 g) at 35°C for 2.5 hours. After the oxidation reaction,

144   DI water (77.0 mL) was introduced into the suspension and the mixture was left to react for

145   an additional two hours at room temperature. To complete the oxidation, H$_2$O$_2$ (30%) (5 mL)

146   was added to the dispersion and the formation of a brilliant yellow color was observed. The

147   dispersion was left to rest for two days, and the precipitate was recovered by centrifugation

148   (12,000 x *g*, 4 °C, for 20 minutes). The resulting material was washed with HCl (10% v/v)

149   and DI water to remove any traces of chemicals. The graphite oxide was resuspended in DI

150   water and additionally purified by dialysis (3,500 Da membranes, Spectrum Laboratories,

151   Inc., CA, USA) for three or four days. The final brown suspension was frozen in liquid

152   nitrogen, dried by lyophilization, and stored at room temperature.

153   GOAg nanocomposites were synthesized by employing Tollens' modified method,

154   which is based on the complexation of Ag^+ ions with NH_4OH and further reduction using

155   saccharides [29]. To prepare GOAg nanocomposites, GO (12.5 mg) was dispersed in DI

156   water (35 mL) and bath-sonicated (Aquasonic Model 150T) for 30 minutes. $AgNO_3$ (8.65

157   mg) was dissolved in 5 mL of DI water and then combined with a 50 mM NH_4OH solution (5

158   mL). The resulting solution was stirred for 10 minutes. Then, the silver solution was

159   introduced to the prior GO dispersion and the mixture was bath-sonicated for an additional 20

160   minutes. Immediately after sonication, 5 mL of a glucose solution (100 mM) was added by

161   drops. The reaction was conducted overnight at room temperature. After synthesis

162   completion, the color of the suspension changed from brown to green-blue, indicating the

163   nanocomposite formation. To remove the excess of chemical residues, the GOAg

164   nanocomposite suspension was purified by dialysis (3,500 Da membranes, Spectrum

165   Laboratories, CA, USA) for three hours and further dried by lyophilization.

166   GOAg nanocomposites were characterized by UV-Vis spectroscopy (Hewlett Packard

167   8453 spectrophotometer) through the detection of the plasmon absorption band. To evaluate

168   the content of silver in the GOAg sample, thermogravimetric analysis (TGA) was carried out

169   using a Setaram Setsys 1750 TG-DTA. The thermogravimetric curves were obtained from

170   100 to 800°C at a heating rate of 5°C min^{-1} under synthetic air. The morphological properties

171   of GO and GOAg nanocomposites were investigated by transmission electron microscopy

172   (TEM) at an accelerating voltage of 200 kV (FEI Tecnai Osiris).

173   *2.3 Functionalization of TFC membranes with GO and GOAg nanocomposites*

174   The polyamide active layer of thin-film composite (TFC) membranes was

175   functionalized with GO or GOAg using a well-stablished method adapted from previous

176   studies [15, 16]. Pristine TFC membranes were placed in frames and sealed with clips to

177   avoid any leakage. With only the active (top) surface exposed, the membranes were kept on

178   an orbital shaker at 60 rpm at room temperature throughout the functionalization procedure.

179   GO and GOAg nanocomposites were chemically bound to the TFC membranes using

180   EDC and NHS as crosslinks. The entire functionalization process can be divided into three

181   steps. The first step is the activation of the native carboxylic functional groups on TFC

6

182   membranes. For this, EDC (4.0 mM) and NHS (10.0 mM) were dissolved in 10 mM MES

183   buffer (pH 5.0) and left to react with the membrane surface for two hours. Next, the solution

184   was removed and the membrane surface was rinsed twice with DI water. In the presence of

185   EDC and NHS, the native carboxyl functionalities on the membrane surface were converted

186   to reactive ester groups. In the second step, the activated carboxyl groups were reacted with

187   ethylene diamine (ED) (10 mM) in a 0.15 M NaCl and 10 mM HEPES buffer (pH 7.5) for

188   one hour to yield an amine-terminated membrane surface. The membrane surface was then

189   rinsed twice with DI to remove unbound ED.

190   The third step comprises the activation of the carboxylate groups on GO and GOAg by

191   EDC and NHS, as described earlier for the pristine TFC membrane. Twenty-five milliliters of

192   the GO and GOAg dispersions (250 µg mL^{-1}) were diluted with 20 mL of 10 mM MES buffer

193   (pH 6). EDC (1.5 mM) and NHS (2.5 mM) were dissolved in 5 mL of MES buffer (pH 6.1)

194   and slowly poured into the GO and GOAg dispersions. The system was kept stirring for 30

195   minutes at room temperature. EDC and NHS decreased the buffer pH to 5.5-5.8. Before

196   contact with the membrane surface, pH was adjusted to 7.2 using a sodium hydroxide

197   solution (1 M). After activation, the ED-functionalized membrane coupons were brought into

198   contact with 20 mL of the activated GO and GOAg samples, and the system was gently

199   stirred at room temperature for three hours. The intermediate reactive esters on GO and

200   GOAg react with the primary amine functional groups, thus irreversibly binding the

201   nanomaterials to the membrane surface. At the end of the reaction, the membranes were

202   rinsed to wash out the unbound materials and restore the unreacted carboxyl groups. The TFC

203   membranes modified with GO or GOAg are referred to as TFC-GO and TFC-GOAg,

204   respectively.

205   *2.4 Membrane characterization*

206   The presence of GO and GOAg nanocomposites on the membrane surface was

207   confirmed by scanning electron microscopy (SEM) using an XL-Philips scanning electron

208   microscope. A Cressington (208 carbon) sputtering machine was applied to coat the sample

209   with a thin layer (10-20 nm) of carbon. Images were taken at an acceleration voltage of 10

210   kV. Energy dispersive spectroscopy (EDS) was utilized to detect the presence of silver.

211   Raman spectroscopy (Horiba Jobin Yvon HR-800) was also used to characterize the

212   functionalization of TFC membranes with GO or GOAg. At least five random locations on

213   the membrane surface were scanned and the Raman spectra were recorded utilizing a 532 nm

214   laser excitation.

215   Surface hydrophilicity was investigated through static contact angles (Theta Lite

216   Optical Tensiometer TL100). Considering the intrinsic variability of this technique, eight

217   measurements were taken at random spots on several dried membrane coupons. Membrane

218   surface roughness was analyzed by atomic force microscopy (AFM, Bruker, Digital

219   Instruments, Santa Barbara, CA, USA) in a peak force tapping mode. Scanasyst-air silicon

220   tips, coated with reflective aluminum, were employed (Bruker Nano, Inc., Camarillo, CA,

221   USA). The tip has a spring constant of 0.4 N m^{-1}, resonance frequency of 70 kHz, tip radius

222   of 2 nm, and cantilever length of 115 µm and width of 25 µm. All images were captured from

223   six randomly selected areas on each membrane coupon. The average surface roughness was

224   calculated from three different measurements for each membrane sample (pristine and

225   modified).

226   The transport properties of the membrane were determined in a cross-flow FO filtration

227   system according to a four-step method reported in our previous publication [30]. Briefly, the

228   experiments were carried out in a laboratory-scale cross-flow forward osmosis unit. Speed

229   gear pumps (Cole-Parmer, Vernon Hills, IL, USA) were used to circulate the solutions in a

230   cross-flow velocity of 9.56 cm s^{-1}. DI water and NaCl solutions were used as feed and draw

231   solutions, respectively. A water bath (Neslab, Newington, NH, USA) was applied to keep the

232   temperature of both feed and draw solutions constant at 25 ± 0.5°C. Water flux was

233   determined by monitoring the rate of change in weight of the draw solution. NaCl

234   concentration in the feed solution was measured at regular intervals using a conductivity

235   meter (Oakton Instruments, Vernon Hills, IL, USA) in order to quantify the reverse NaCl

236   flux. Four different stages were employed by changing the NaCl concentrations of the draw

237   solution. These measurements allowed for the determination of the water permeability

238   coefficient (*A*), the salt permeability coefficient (*B*), and the membrane structural parameter

239   (*S*). These parameters were adjusted to fit the experimental data of water and reverse salt

240   fluxes to the corresponding governing equations.

241   ***2.5 Assessing antimicrobial activity of functionalized TFC membranes***

242   *Pseudomonas aeruginosa* (ATCC 27853) was used as the model bacteria. *P.*

243   *aeruginosa* cells were cultivated on Lauria-Bertani (LB) broth overnight at 37°C. The

244   bacterial cells were then diluted (1:50) in fresh LB medium until they reached an optical

245   density of 1.0 at 600 nm (OD$_{600nm}$) (~2 hours), which corresponds to a concentration of ~10^9

246   CFU mL^{-1}. The bacterial suspension was then washed twice with saline solution (0.9%) by

247   centrifugation for 2 minutes at 10,000 rpm to remove the excess growth medium constituents.

248   The resulting suspension was diluted to 10^8 CFU mL^{-1} in a sterile isotonic solution (NaCl,
249   0.9% w/v).

250   A plate-counting method was employed to evaluate the inactivation of bacteria by the
251   GO and GOAg functionalized membranes. TFC, TFC-GO, and TFC-GOAg membranes were
252   cut in round coupons of approximately 1.5 cm^2 and placed on plastic holders. These plastic
253   holders only allowed the membrane top surface to contact the bacterial suspension. The
254   membrane surface was in contact with the bacterial solution (2 mL) for three hours at room
255   temperature. The bacterial suspension was then discarded and coupons were rinsed with
256   sterile 0.9% saline solution to remove the non-adhered bacteria. The membrane coupons were
257   transferred to 50 mL falcon tubes containing 10 mL 0.9% saline solution. Subsequently, the
258   falcon tubes were bath-sonicated (26 W L^{-1}, FS60 Ultrasonic Cleaner) for 15 minutes to
259   detach the bacterial cells from the membrane surface. Aliquots were collected, sequentially
260   diluted in 0.9% saline solution, and spread on LB agar plates. Plates were incubated
261   overnight at 37°C.

262   The morphology of the attached cells was imaged by SEM. The bacteria cells attached
263   to the membrane coupons were fixed using Karnovsky's solution (4% paraformaldehyde and
264   5% glutaraldehyde diluted in 0.2 M cacodylate buffer pH 7.4) for three hours. The cells were
265   consecutively dehydrated by immersing the membrane coupons in water-ethanol (50:50,
266   30:70, 20:80, 10:90, and 100% ethanol) and ethanol-freon solutions (50:50, 25:75, and 100%
267   freon) for 10 minutes. After the sequential dehydration steps, the fiber coupons were dried
268   overnight in a desiccator at room temperature. The samples were then sputter-coated with 10
269   nm carbon (Cressington coater, 208 carbon), and the bacteria cells were imaged by SEM (XL
270   series-Philips) operating at an acceleration voltage of 10 kV.

271   *2.6 Membrane biofouling and biofilm characterization protocols*

272   Biofilm development was evaluated for the pristine TFC, TFC-GO, and TFC-GOAg
273   membranes in a custom-designed cross-flow test cell. *P. aeruginosa* was cultivated as
274   described above and then transferred to a synthetic wastewater composed of 1.2 mM sodium
275   citrate, 0.8 mM NH$_4$Cl, 0.2 mM KH$_2$PO$_4$, 0.2 mM CaCl$_2$·H$_2$O, 0.5 mM NaHCO$_3$, 8.0 mM
276   NaCl, and 0.15 mM MgSO$_4$·7H$_2$O, as previously reported [31]. The initial bacteria
277   concentration in the synthetic wastewater solution was 10^7 cells mL^{-1}. The temperature was
278   kept at 25°C throughout the experiment.

279   At the end of the experiment, the membrane coupons were cut in small pieces (1 cm^2)
280   and placed in individual petri dishes. The samples were rinsed with a 0.9% NaCl solution to
281   remove non-adhered bacteria, and the biofilm was stained with SYTO 9 and propidium iodide
282   (PI) (Live/Dead® BacLight™, Invitrogen, USA). Live and dead cells were stained in green
283   and red, respectively. Concanavalin A (Con A, Alexa Flour® 633, Invitrogen, USA) was used
284   to stain exopolysaccharides (EPS) in blue. The dyes were in contact with the biofilm for at
285   least 20 minutes in the absence of light. Samples were rinsed to remove the excess stain and
286   imaged using a confocal laser scanning microscopy (Zeiss LSM 510, Carl Zeiss, Inc.). Lasers
287   at the wavelength of 488 nm (argon), 561 nm (diode-pumped solid state), and 633 nm
288   (helium–neon) were used to excite SYTO 9, PI, and Con A staining, respectively. Random
289   locations were scanned to obtain representative areas of the biofilm. Intrinsic characteristics
290   such as biofilm thickness and biovolume of live and dead bacterial components of the biofilm
291   were also determined.

292   Biofilm total organic carbon (TOC) and protein concentration were also quantified.
293   For TOC measurements, membrane sub-sections (2 cm × 2 cm) were re-suspended in 24 mL
294   sterile wastewater with 10 µL of 1 M HCl. Samples were then sonicated on ice in three 30-
295   second cycles to remove organic content from the membrane. TOC in the resultant solution
296   was then analyzed using a TOC analyzer (TOC-V, Shimadzu, Japan). TOC concentrations
297   were normalized by membrane sample area. For protein quantification, membrane sub-
298   sections (2 cm × 2 cm) were cut and suspended in 2 mL Eppendorf tubes with 1 mL 1X
299   Lauber buffer (50 mM HEPES (pH 7.3), 100 mM NaCl, 10% sucrose, 0.1% CHAPS, and 10
300   mM DTT) and probe sonicated on ice (three 30-second cycles) using an ultra-cell disruptor.
301   The membrane was then removed and cell extracts were centrifuged at 12,000 rpm for 10
302   minutes to remove detritus matter. The supernatant was then collected for protein
303   quantification using a BCA protein assay kit (Thermo Scientific, IL).

3. Results and Discussion

3.1 Physicochemical characteristics of GO and GOAg nanocomposites

306   The chemical exfoliation of graphite produces a brown dispersion composed of single-
307   layer graphene oxide (GO) sheets (**Figure 1A**). A typical GO sample characteristically has a
308   wide size distribution. GO average size is dependent on several factors such as time of
309   reaction, the graphite precursor, and the concentration and type of oxidizing agent used
310   during sample preparation. The SEM image of an aqueous suspension of our prepared GO
311   (**Figure 2**) shows the presence of flat sheets with an average area of 0.36 ± 0.37 µm^2. The

312 average size of GO sheets has been shown to influence their reactivity, in particular the
313 cytotoxicity to bacterial cells [28, 32].

314

315
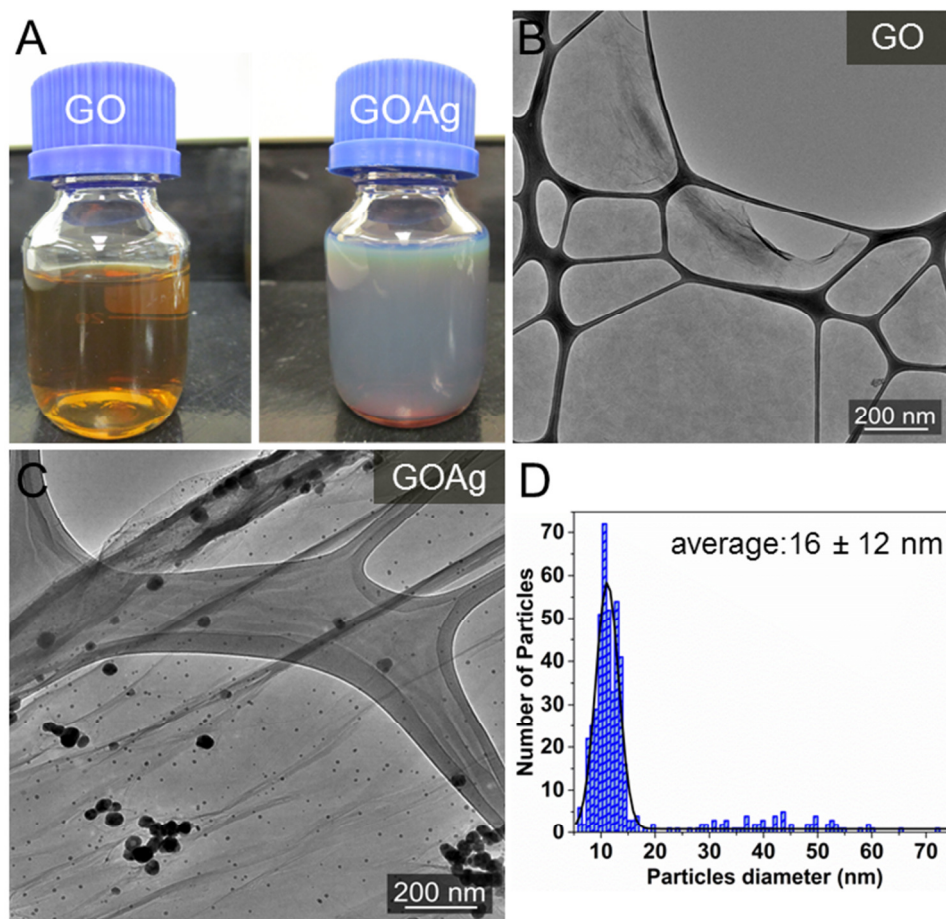
Figure 1: (A) Photographs of bare GO (left) and GOAg nanocomposites (right) dispersions.
The green-blue color is an indicator of the formation of silver nanoparticles on GO surface.
GOAg nanocomposites were prepared through in-situ reduction of $AgNO_3$ (1 mM) in the
presence of GO sheets (125 µg mL^{-1}). Representative transmission electron microscopy
(TEM) images of (B) GO and (C) GOAg nanocomposites. (D) size distribution of silver
nanoparticles attached to GO surface. Silver nanoparticles revealed an average size of 16 ±
12 nm after counting approximately 200 particles on several TEM images.

323

324   For the preparation of GOAg nanocomposites, GO powder was dispersed in DI water
325 and mixed with the precursor $AgNO_3$. The reaction was conducted at alkaline conditions due
326 to the addition of ammonium hydroxide (NH_4OH); glucose (dextrose) was used as a reducing
327 agent. The change in color from brown to green-blue was an indicator of the decoration of
328 GO sheets with AgNPs (**Figure 1A**). Previous studies have reported the use of sugar to
329 reduce Ag^+ ions to silver nanoparticles [29]. This method is widely known as the *Tollens*
330 reaction. The mechanism involves the interaction of Ag^+ ions with NH_4OH to form

331   intermediate species $(Ag(NH_3)_2)^+$ that are then reduced to nanoclusters upon contact with the

332   sugar molecules [33]. It is worth mentioning that the reducing property of monosaccharides,

333   such as glucose, is attributable to the presence of free aldehyde or ketone functional groups

334   on the sugar molecules. In comparison to many of the processes already reported in the

335   literature, the *Tollens* method is advantageous since it applies a non-toxic and an

336   environmental friendly molecule as a reducing agent. Moreover, the chemical reaction does

337   not require high temperatures or the use of aggressive organic solvents [23, 24, 34, 35].

338   Given the change in color, a UV-Vis spectrum was recorded to indirectly confirm the

339   formation of silver nanoparticles in the GO dispersion. The plasmon band (~ 440 nm) on the

340   UV-Vis spectrum of GOAg nanocomposites suggests the presence of nanoparticles in the GO

341   dispersion (**Figure S1A**) [23, 25]. The additional absorption peaks at approximately 230 and

342   305 nm are associated with π-π* transitions of C-C aromatic and n-π* transitions of C=O

343   bonds of GO sheets, respectively [23, 35, 36]. X-ray diffraction (XRD) analyses have also

344   been applied as a way to demonstrate the crystallographic features of the silver nanoparticles

345   deposited on GO sheets. For GOAg nanocomposites, the X-ray diffraction spectrum (**Figure**

346   **S1B**) displays peaks at 38.3, 44.3, 64.4, and 77.3° that correspond to the 111, 200, 220, and

347   311 crystalline planes of AgNPs, respectively [36]. Thermogravimetric analysis was carried

348   out to investigate the thermal decomposition pattern of both GO and GOAg (**Figure S1C**).

349   TGA curves also provide information about the silver content in the GOAg sample [23, 24].

350   The residues above 600°C indicate that the relative content of silver is approximately 10 wt

351   % of the total GOAg nanocomposites (**Figure S1C**).

352
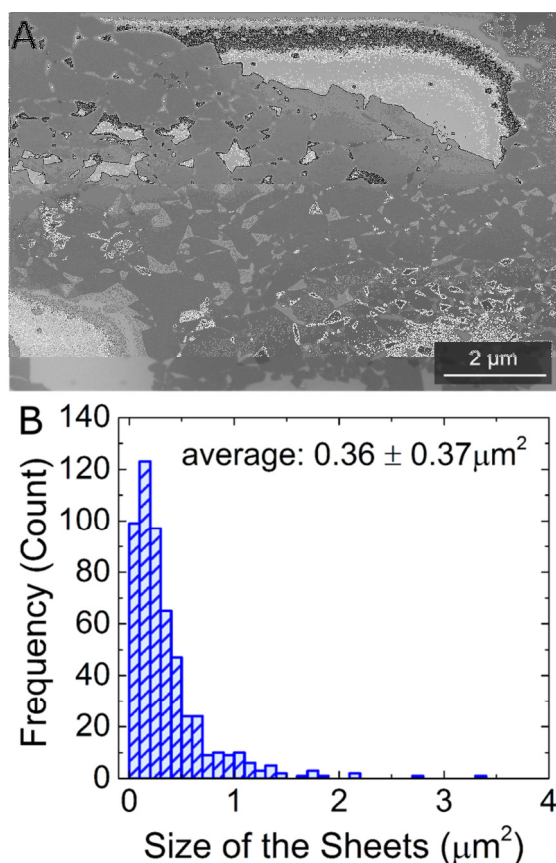
Figure 2: (A) Scanning electron microscopy (SEM) image of graphene oxide (GO) sheets.
Graphene oxide dispersion was deposited on a silicon wafer and the images were taken at an
acceleration voltage of 15 kV. (B) size distribution of GO sheets; the average size was
estimated by measuring the area (μm^2) of multiple GO sheets using the software ImageJ.

357

The decoration of GO sheets with AgNPs was confirmed by transmission electron
microscopy (TEM), as shown in **Figure 1C**. The AgNPs appeared as black dots distributed
throughout the graphene surface with an average size of 16 ± 12 nm (**Figure 1D**). Both GO
and GOAg nanocomposites showed a wrinkled and paper-like morphology on the TEM
images (**Figures 1B and C**). Since particles were not found detached from GO sheets, we
surmise the nucleation occurs preferentially on the graphene surface. The negatively charged
oxygen-containing functional groups on GO likely offer nucleation sites for the Ag$^+$ ions via
electrostatic interaction [23, 35]. Once adsorbed on GO sheets, Ag$^+$ ions can be reduced to
Ag^0 nanoparticles in the presence of a reducing agent. The physicochemical characteristics of
GOAg nanocomposites may differ depending on the degree of oxidation of GO sheets and the
initial concentration of silver utilized [37, 38].

369

370

3.2 GO and GOAg sheets are covalently bound to the membrane surface

372   The binding of GO and GOAg nanocomposites to TFC membranes was developed
373   through a reaction mediated by EDC and NHS. The polyamide layer of TFC membranes
374   possesses native carboxyl groups that can react with ethylene diamine (ED) via EDC and
375   NHS to yield an amine-terminated surface. Similarly, the carboxyl groups on GO layer are
376   activated when exposed to EDC and NHS in a buffered solution. During this activation, the
377   carboxyl groups on GO are converted to intermediate esters that readily react with amine
378   groups on ED-functionalized TFC membranes. GO and GOAg sheets are covalently linked to
379   the polyamide layer through the formation of an amide bond between carboxyl groups of GO
380   and the amine groups on ED-functionalized TFC membranes. A scheme in **Figure 3**
381   illustrates the reaction mechanism involved in the binding of GOAg sheets to the membrane
382   surface.
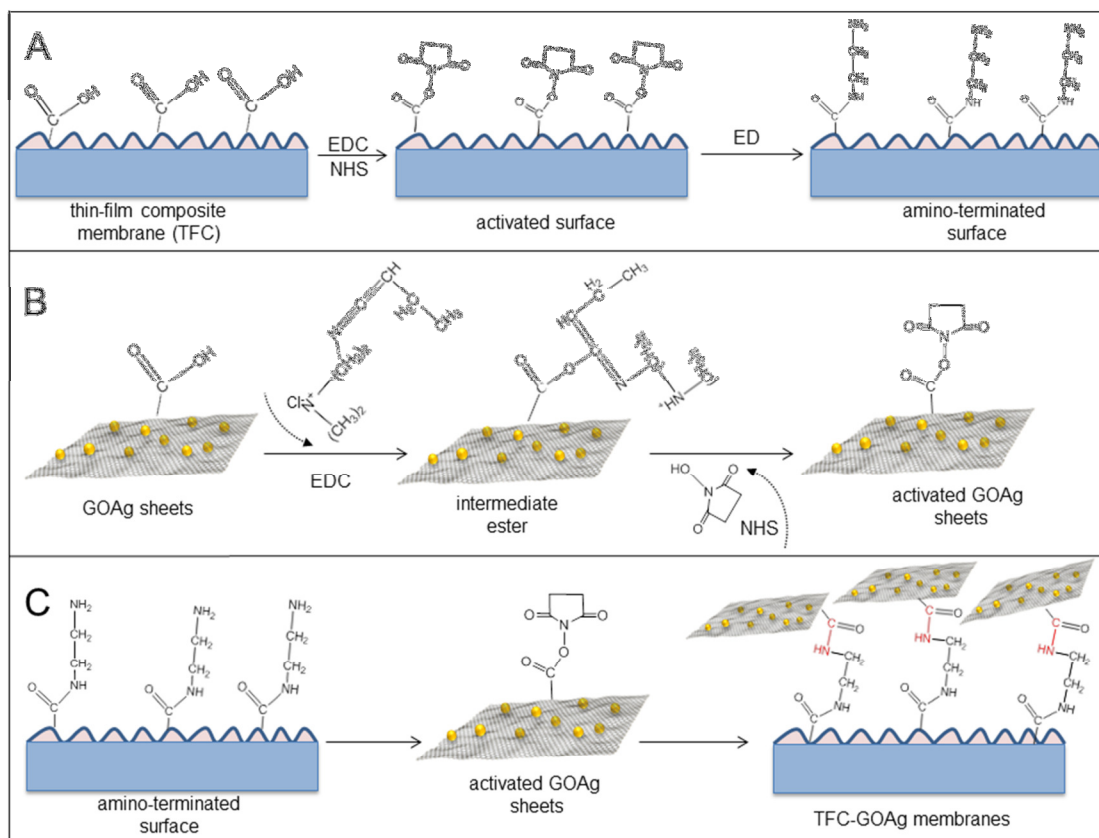
383

384   **Figure 3**: Scheme illustrating the three-sequential steps (A, B, and C) for binding GOAg
385   sheets to the surface of thin-film composite membranes. (A) Carboxylic groups on the
386   polyamide layer are converted into primary amine groups; the native carboxylic groups are
387   activated by EDC and NHS to generate a highly reactive ester that spontaneously reacts with
388   ethylenediamine (ED) to allow an amine-terminated surface. (B) Carboxylic functional
389   groups on GOAg sheets are activated in presence of EDC and NHS. (C) The amine-

390 terminated TFC membrane contacts the activated GOAg sheets. This reaction leads to the
391 binding of graphene sheets through the formation of an amide bond.

392   SEM imaging of the pristine membrane surface shows a ridge-and-valley morphology
393 characteristic TFC membrane (**Figure 4A**) [13, 15, 16]. The areas where the polyamide layer
394 was modified with GO or GOAg sheets appeared as dark spots on the membrane surface
395 (**Figures 4B and C**). No such dark spots are present on the SEM images of pristine
396 membranes (**Figure 4A**). The rough surface of the polyamide layer seems to be covered by
397 GO or GOAg nanosheets and small bright features (~50 nm) were detected on the surface of
398 TFC-GOAg membranes (**Figure 4C**). Energy dispersive spectroscopy (EDS) spectrum
399 acquired directly from those bright spots revealed a peak at 4.0 keV that is attributable to
400 silver (**Figure 4D**). A visual inspection indicated that TFC membranes did not present drastic
401 changes in color after binding GO or GOAg nanocomposites.

402
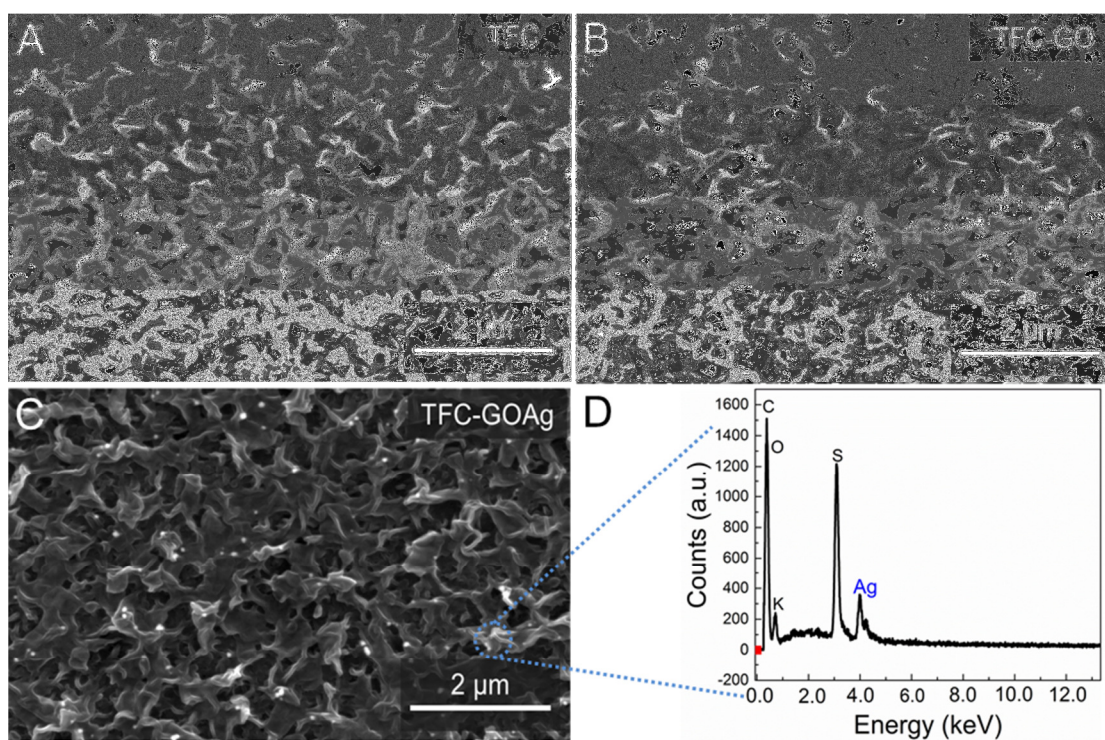
404 **Figure 4**: Scanning electron microscopy (SEM) images of the polyamide active layer of (A)
405 pristine TFC, (B) TFC-GO, and (C) TFC-GOAg membranes. Images were taken at an
406 acceleration voltage of 10 kV. (D) Energy dispersive spectroscopy (EDS) spectrum of bright
407 dots on the surface of TFC membranes modified with GOAg. The peak at 4.0 keV is
408 commonly ascribed to the presence of silver.

409   In addition to SEM imaging, GO and GOAg-modified membranes were characterized
410 by Raman spectroscopy (**Figure 5**). The functionalization of TFC membranes with both
411 nanomaterials was indirectly confirmed through changes in the intensity ratio between the

15

412 peaks at 1148 and 1620 cm^{-1} (I_{1148}/I_{1620}), as reported in our previous publication [16]. Among

413 several absorption peaks, Raman spectrum of TFC membranes is particularly characterized

414 by the presence of symmetric C-O-C stretching (~1148 cm^{-1}) and phenyl ring vibration

415 (~1590-1620 cm^{-1}) [39]. It is already well known that bare GO displays two reference peaks

416 at 1350 cm^{-1} (D band) and 1590 cm^{-1} (G band) in the Raman spectrum [40]. With the binding

417 of GO and GOAg nanocomposites, the intensity of the peak at 1148 cm^{-1} is expected to

418 decrease, whereas the intensity of the peak at 1620 cm^{-1} is likely to increase due to the

419 contribution of the G band from GO sheets. Comparison of multiple functionalized

420 membranes demonstrated that the I_{1148}/I_{1620} ratio for TFC-GO (0.30 ± 0.12) and TFC-GOAg

421 (0.26 ± 0.12) was significantly decreased ($p < 0.005$) in comparison to pristine TFC

422 membranes (0.93 ± 0.20) (**Figure 5**). The noticeable decrease in the I_{1148}/I_{1620} ratio is an

423 additional confirmation of the successful functionalization of TFC membranes with GO or

424 GOAg nanosheets.
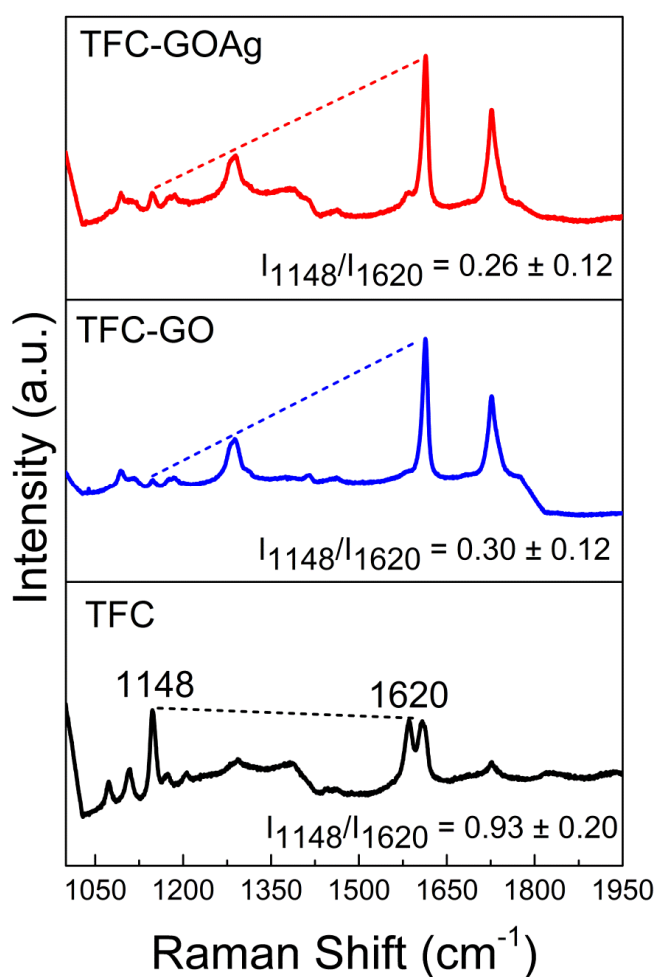
425

426 **Figure 5**: Raman spectra of the TFC (black), TFC-GO (blue), and TFC-GOAg (red)
427 membranes. The ratio between the intensity of the bands at 1148 and 1620 cm^{-1} was used to

428 identify the presence of GO and GOAg on the membrane surface. The I_{1148}/I_{1620} average
429 values are a result of at least five random measurements at different locations on each
430 membrane surface.
431

3.3 GO and GOAg sheets impact membrane surface properties

433   AFM images (**Figure 6**) were taken to evaluate changes in the polyamide roughness

434 after modification with GO or GOAg. A significant decrease in surface roughness was

435 observed for TFC-GO as compared to pristine TFC membranes. On the other hand, in

436 comparison with the unmodified control, TFC-GOAg membranes presented only a slight

437 decrease in roughness. The covering of the polyamide ridge-and-valley features by GO sheets

438 might be the cause of the reduction in surface roughness observed for TFC-GO membranes

439 [15]. TFC, TFC-GO, and TFC-GOAg membranes presented a root mean squared (*Rq*) surface

440 roughness of 84.8 ± 5.3, 49.7 ± 6.5, and 77.9 ± 6.2 nm, respectively (**Figure 7A**). This result

441 may suggest that GOAg sheets provided a less effective coating of the membrane surface. It

442 is likely that GO sheets are partially reduced in contact with the reducing agent during the

443 synthesis of GOAg. As a result, GOAg nanocomposite dispersions are less stable and

444 aggregate, which could lead to a decreased diffusion rate of the GOAg sheets towards the

445 membrane surface during modification. As a consequence, the binding of GOAg sheets is

446 probably minimized in comparison to that expected for pristine GO sheets. Furthermore, the

447 AgNPs themselves, especially the aggregates, could increase the roughness for TFC-GOAg

448 compared to TFC-GO membranes.

449

450

17
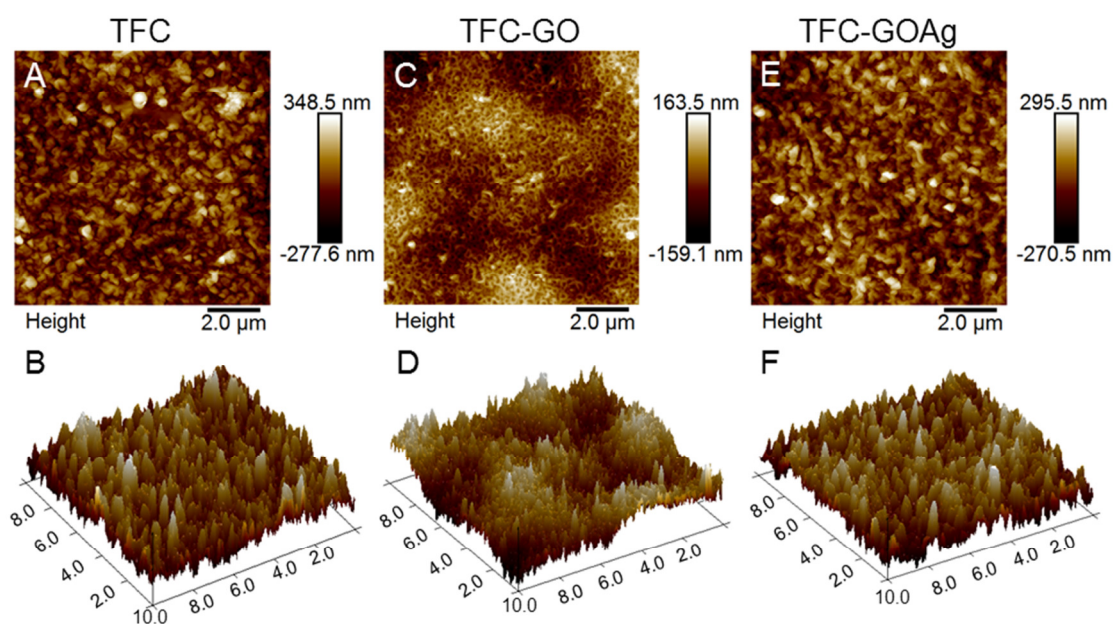
Figure 6: Atomic force microscopy (AFM) images of (A, B) pristine TFC, (C, D) TFC-GO, and (E, F) TFC-GOAg membranes. The units are in micrometers (μm).

Changes in surface hydrophilicity were investigated through static water contact angle measurements (**Figure S2**). However, no significant differences in contact angle were noticed after functionalization of TFC membranes with either GO (32.6 ± 2.8°) or GOAg sheets (33.8 ± 6.2°), despite the large amount of hydrophilic, oxygen-containing functional groups on the graphene sheets. One reason for this observation is the already relatively very low contact angle of the pristine TFC membranes (38.1 ± 1.9°).

*3.4 Functionalization with GOAg nanocomposites does not affect membrane transport properties*

One of the greatest challenges of modifying the surface of TFC membranes is to ensure that water permeability (*A*) and salt selectivity (*B*) are not affected by the binding of polymeric molecules or nanomaterials. **Figure 7B** summarizes the *A*, *B*, and *S* parameters for TFC, TFC-GO, and TFC-GOAg membranes. We observed that the *A* and *B* coefficients did not significantly change with the binding of GO or GOAg to the membrane surface ($p >$ 0.05), even though TFC-GOAg presented a small decrease in the water permeability coefficient *A* compared to the unmodified membrane (**Figure 7B**). The salt permeability coefficient *B* slightly increased from 1.33 ± 0.21 L m^{-2} h^{-1} for the pristine membrane to 1.64 ± 0.32 and 1.59 ± 0.21 L m^{-2} h^{-1} for TFC-GO and TFC-GOAg membranes, respectively. As expected, **Figure 7B** also reveals that the membrane structural parameter *S* of the pristine TFC membrane did not change by our modification procedure. These results indicate that the functionalization with GO or GOAg does not impact the transport properties of the membrane polyamide layer. This result is consistent with our previous work, where the modification of RO TFC membranes with pristine GO did not change the membrane transport properties [16, 41]. Similar observations have also been reported for TFC RO membranes modified with multiple layers of GO sheets [42]. This low impact of GO on the membrane performance is probably due to its atomic thickness and hydrophilic nature. **Table S1** presents one full set of experimental data (measured water and reverse salt fluxes and relevant coefficients of determination, R^2) for the TFC, TFC-GO, and TFC-GOAg membranes, used for the calculation of *A*, *B*, and *S*.

485

486
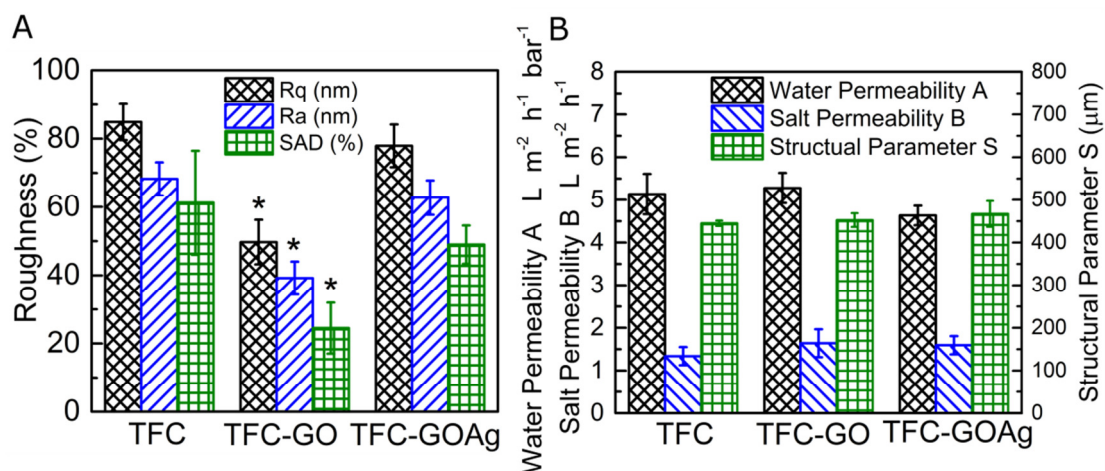
Figure 7: (A) Surface roughness determined by atomic force microscopy (AFM) for pristine TFC, TFC-GO, and TFC-GOAg membranes. The roughness parameters extracted from AFM images are root-mean-square value (Rq), average roughness (Ra), and percent surface area difference (SAD %). The roughness data were collected from at least five different areas on the membrane surface. (B) Transport and performance properties of TFC, TC-GO, and TFC-GOAg membranes: water permeability coefficient *A*, salt (NaCl) permeability coefficient *B*, and structural parameter *S*. Asterisks above bars indicate that the TFC-GO membrane roughness parameters were significantly different ($p < 0.01$) than the corresponding values of the other two membranes.

3.5 Bacterial attachment and viability are significantly suppressed by GOAg

Antimicrobial activity was first evaluated after exposing the membrane surface to *P. aeruginosa* cells for three hours. In comparison to pristine TFC, the TFC-GO membrane displayed no toxic effect towards *P. aeruginosa* (**Figure 8A**). TFC-GOAg membrane, on the other hand, exhibited a bacterial inactivation rate of around 80% against *P. aeruginosa*, relative to the non-modified TFC membranes. In other words, the number of viable cells on TFC-GOAg was significantly lower than that of the unmodified control, implying that functionalization with GOAg imparted a strong antimicrobial activity to the membrane surface.

507
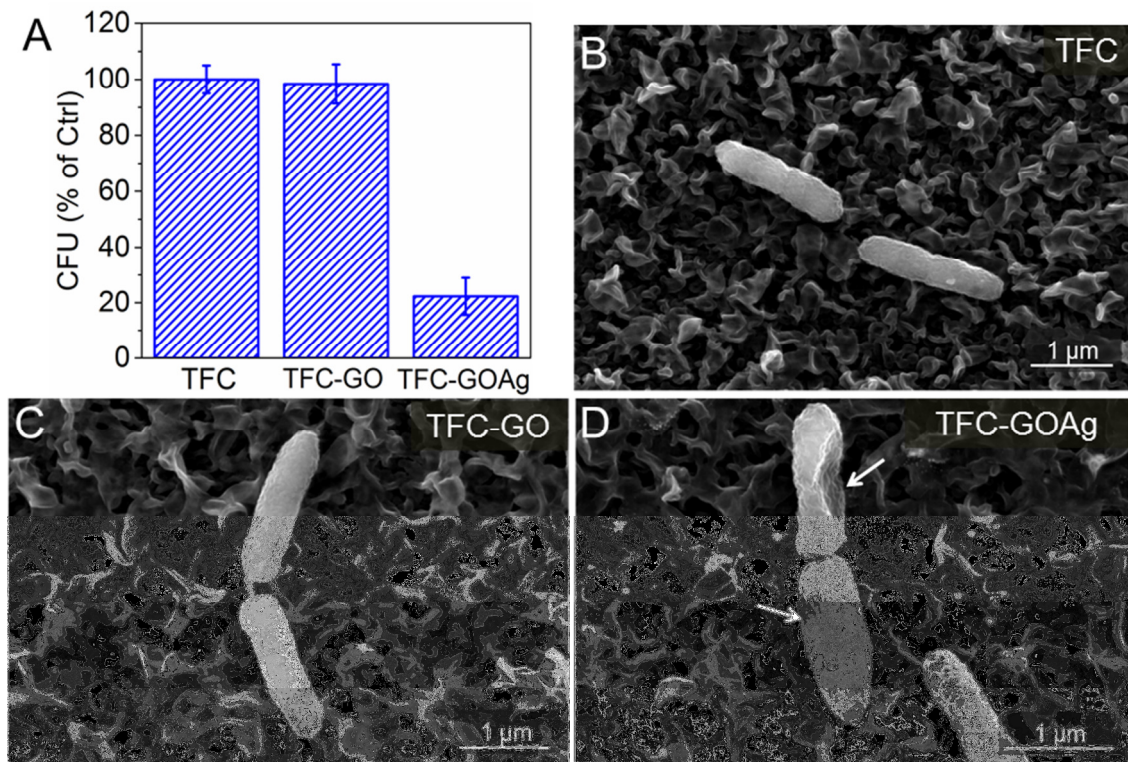
Figure 8: (A) Viable cells of *P. aeruginosa* after three hour contact with the surface of pristine and graphene modified membranes. The viability of *P. aeruginosa* cells is expressed as the percentage of colony-forming units (CFU) relative to the pristine TFC control membrane. Standard deviation error bars were calculated from three independent replicates. Scanning electron microscopy (SEM) images of bacteria cells attached to the polyamide active layer of (B) pristine TFC, (C) TFC-GO, and (D) TFC-GOAg membranes. Severe morphological damage for bacteria cells on TFC-GOAg is highlighted by white arrows on the image (panel D). SEM images were taken at an accelerating voltage of 10 kV.

Morphological characteristics of adhered bacterial cells were examined by SEM (**Figures 8B, C, and D**). The microbial cells attached to pristine TFC membrane remained intact after exposure. However, SEM images clearly demonstrated that *P. aeruginosa* cells on TFC-GOAg membrane surface were severely damaged, as indicated by white arrows in **Figure 8D**. Upon contact with TFC-GOAg surface, the adhered cells revealed a flattened and shrunken morphology. The loss in morphological integrity is likely caused by the presence of AgNPs, and the mechanism of toxicity can be explained by both release of toxic Ag^+ ions and direct contact with the AgNPs on the membrane surface [25, 43]. The high affinity of silver for thiol (-SH) functional groups of proteins may damage the stability and architecture of the bacterial cell wall through the generation of holes and vacancies [44, 45]. Disruption of cell wall structure could irreversibly affect the transport of nutrients, thus inactivating the bacterial cells.

20

3.6 GOAg nanocomposite functionalized membranes exhibit reduced biofouling rate.

530

531   The anti-biofouling properties of TCF and TFC-GOAg membranes were investigated

532 by allowing *P. aeruginosa* cells to grow on the membrane surface for 24 hours in a dynamic

533 cross-flow biofouling test. One of the consequences of biofilm formation on TFC membranes

534 is the decrease in permeate water flux. As shown in **Figure 9A**, the development of biofilm

535 on pristine TFC membrane resulted in a flux decline of approximately 50%. However, when

536 TFC membrane is functionalized with GOAg nanocomposites, the flux decline is

537 significantly reduced. The difference in the water flux behavior is attributable to differences

538 in the structure and composition of the biofilms on the pristine TFC and TFC-GOAg

539 membranes.

540   To obtain information about the biofilm properties, the biofouled membranes were

541 characterized by confocal microscopy. **Figures 9 B and D** show representative CLSM

542 images of the biofilm prior and after the functionalization of TFC membranes with GOAg

543 nanosheets, respectively. Dead cells, represented in red color, are more abundant on TFC-

544 GOAg (**Figure 9D**) than on TFC-GO or pristine TFC membranes (**Figures 9B and C**). The

545 dead cell region reached the top layer of the biofilm on the TFC-GOAg membrane, indicating

546 that direct contact with the GOAg nanocomposite was not required and that silver ions could

547 leach and diffuse to the upper cell layers. Therefore, the addition of Ag in a GOAg

548 nanocomposite played a key role in mitigating biofilm development on TFC membranes.
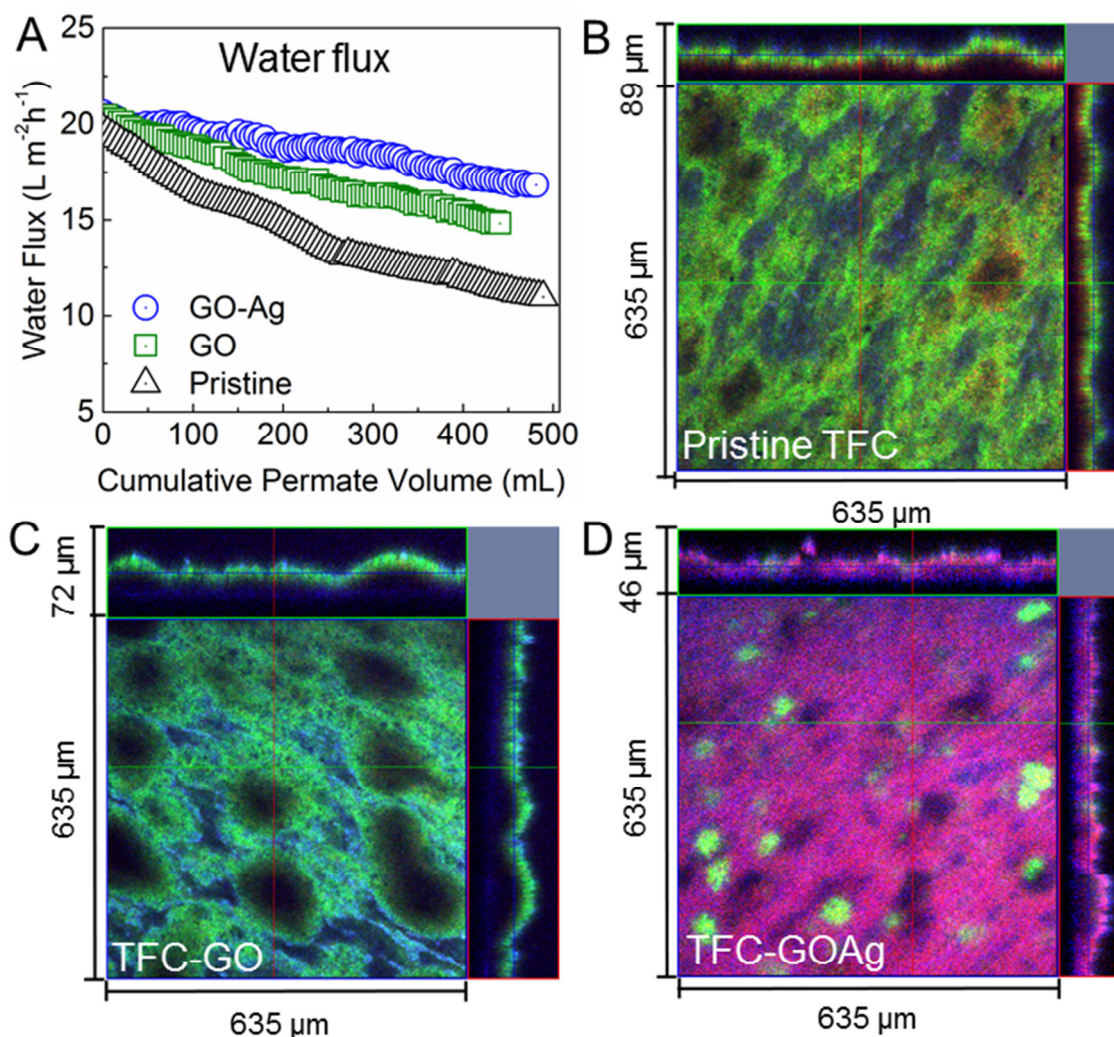
549

550 **Figure 9**: (A) Water flux decline caused by the formation of biofilm during biofouling
551 experiments in a cross-flow cell. Water flux decline data were obtained from two independent
552 duplicates. The biofouling experiments were conducted using synthetic wastewater with
553 glucose as a carbon source. Temperature and cross-flow velocities were kept at 25°C and
554 9.56 cm s^{-1}, respectively. To achieve the initial water flux of 20 L m^{-2} h^{-1}, we used NaCl draw
555 solution in the range of 0.4 to 0.7 M. Under these conditions, the reverse salt fluxes for
556 pristine TFC, TFC-GO, and TFC-GOAg membranes were 110, 115, and 145 mmol·m^{-2}·h^{-1},
557 respectively. Confocal laser scanning microscopy (CLSM) images of *P. aeruginosa* biofilm
558 developed on the polyamide active layer of (B) pristine TFC, (C) TFC-GO, and (D) TFC-
559 GOAg membranes. The biofilm was grown after 24-hour biofouling runs as described in (A).
560 Live cells, dead cells, and exopolysaccharides were stained with Syto 9 (green), propidium
561 iodide (red), and Con A (blue) dyes, respectively.

562

563   **Table 1** summarizes the biofilm properties for TFC, TFC-GO, and TFC-GOAg

564 membranes. For instance, the biofilm on TFC-GOAg membrane was almost two times

565 thinner than that on the pristine TFC membrane. Furthermore, the live cell biovolume (μm^3

566 μm^{-2}) on TFC-GOAg was decreased by almost 50% compared to the non-modified TFC

567 membrane. The lack of antimicrobial activity for TFC-GO membrane is explained by the
568 relatively large size of the GO sheets [28]. The results observed from confocal imaging are in
569 accordance with the CFU counts reported in Figure 8A, where pristine TFC and TFC-GO
570 membranes exhibited similar antimicrobial properties. The biofilm contents of protein and
571 total carbon were also drastically reduced after modification of TFC membranes with GOAg
572 nanocomposites. The total protein mass was diminished from 18.7 ± 2.5 to 9.1 ± 6.2 pg μm^{-2}
573 after binding GOAg sheets to the membrane surface (**Table 1**).

574   Our findings suggest that bacterial growth on the TFC membrane surface was strongly
575 inhibited by GOAg nanocomposites. The decrease in the number of live cells on the TFC-
576 GOAg membrane led to a significant reduction in biofilm thickness, live cell biovolume, and
577 EPS production (**Table 1**). Our results demonstrate that the development of anti-biofouling
578 TFC membranes can benefit from the physicochemical and biological properties of GOAg
579 nanocomposites. Recognizing that the antimicrobial activity of GOAg nanocomposites is
580 partially dependent on the release of Ag^+ ions, their anti-biofouling properties can be
581 improved by maximizing membrane coverage and/or by tuning the size, shape, and content of
582 AgNPs in the GOAg nanocomposites.

583

Table 1: Characteristics of *P. aeruginosa* biofilm grown on pristine TFC, TFC-GO, and TFC-GOAg membranes after 24 hours. All parameters were determined from confocal laser scanning microscopy (CLSM) images.

Operating condition	Average biofilm thickness (μm) [a]	"Live" cell biovolume ($\mu m^3\ \mu m^{-2}$)	"Dead" cell biovolume ($\mu m^3\ \mu m^{-2}$)	EPS biovolume ($\mu m^3\ \mu m^{-2}$)	Total protein mass (pg μm^{-2})[b]	TOC biomass (pg μm^{-2}) [b]
Pristine TFC	89 ± 5	21.2 ± 4.1	12.1 ± 2.3	20.9 ± 2.2	18.7 ± 2.5	1.57 ± 0.05
TFC-GO	72 ± 2	27.2 ± 5.1	12.1 ± 2.3	12.3 ± 3.6	12.1 ± 4.5	1.11 ± 0.03
TFC-GOAg	46 ± 3	12.5 ± 5.1	29.6 ± 1.1	8.3 ± 3.6	9.1 ± 6.2	0.82 ± 0.07

[a] biofilm thickness and biovolume were averaged, with standard deviations calculated from ten random samples in duplicated experiments.

[b] TOC and protein biomasses were presented with standard deviations calculated from four measurements by two membrane coupons.

4. Conclusion

In this study, we report the synthesis of GOAg nanocomposites and their further application as antimicrobial agents for the control of biofouling in forward osmosis membranes. GOAg nanocomposites were prepared through a straightforward process whereby silver nanoparticles are in-situ nucleated on GO sheets. The formation of silver nanoparticles on GO sheets is done by using glucose as a reducing agent. The resulting GOAg nanocomposites displayed silver nanoparticles with an average size of 16 nm which were bound irreversibly on the GO surface. Carboxylic groups on GOAg were used as target points to bind the graphene sheets to the amine-terminated polyamide layer. The surface modification of TFC membranes with GO or GOAg nanocomposites was successfully demonstrated by SEM and Raman spectroscopy analyses. We also show that the intrinsic transport properties of TFC membranes were not affected by the modification with GO or GOAg nanocomposites.

Static antimicrobial assays showed that GOAg modified membranes were able to significantly inhibit the attachment of *Pseudomonas aeruginosa* cells. Unlike some previous studies, the membrane modified just with GO showed no toxicity to bacterial cells. In addition, dynamic biofouling experiments performed using a bench-scale FO system demonstrated the anti-biofouling property of membranes modified with GOAg sheets. A massive amount of dead cells can be seen on the confocal images taken from TFC-GOAg membranes. In addition, the biovolume of live cells was substantially decreased for membranes modified with GOAg. Dynamic biofouling experiments also showed that the flux decline due to biofouling development was reduced by 30% after modification of TFC membranes with GOAg nanocomposites. Our results suggest that membrane functionalization with GOAg is a robust platform to yield TFC membranes possessing enhanced biofouling resistance.

5. Acknowledgment

6. REFERENCES

[1] M. Elimelech, W.A. Phillip, The Future of Seawater Desalination: Energy, Technology, and the Environment, Science, 333 (2011) 712-717.

[2] M.A. Shannon, P.W. Bohn, M. Elimelech, J.G. Georgiadis, B.J. Marinas, A.M. Mayes, Science and technology for water purification in the coming decades, Nature, 452 (2008) 301-310.

[3] R.J. Petersen, Composite reverse osmosis and nanofiltration membranes, Journal of Membrane Science, 83 (1993) 81-150.

[4] N.Y. Yip, A. Tiraferri, W.A. Phillip, J.D. Schiffman, M. Elimelech, High Performance Thin-Film Composite Forward Osmosis Membrane, Environmental Science & Technology, 44 (2010) 3812-3818.

[5] J.S. Baker, L.Y. Dudley, Biofouling in membrane systems — A review, Desalination, 118 (1998) 81-89.

[6] M. Herzberg, M. Elimelech, Biofouling of reverse osmosis membranes: Role of biofilm-enhanced osmotic pressure, Journal of Membrane Science, 295 (2007) 11-20.

[7] E. Bar-Zeev, U. Passow, S. Romero-Vargas Castrillón, M. Elimelech, Transparent Exopolymer Particles: From Aquatic Environments and Engineered Systems to Membrane Biofouling, Environmental Science & Technology, 49 (2015) 691-707.

[8] G.-D. Kang, C.-J. Gao, W.-D. Chen, X.-M. Jie, Y.-M. Cao, Q. Yuan, Study on hypochlorite degradation of aromatic polyamide reverse osmosis membrane, Journal of Membrane Science, 300 (2007) 165-171.

[9] G. Ye, J. Lee, F. Perreault, M. Elimelech, Controlled Architecture of Dual-Functional Block Copolymer Brushes on Thin-Film Composite Membranes for Integrated "Defending" and "Attacking" Strategies against Biofouling, ACS applied materials & interfaces, 7 (2015) 23069-23079.

[10] D. Saeki, S. Nagao, I. Sawada, Y. Ohmukai, T. Maruyama, H. Matsuyama, Development of antibacterial polyamide reverse osmosis membrane modified with a covalently immobilized enzyme, Journal of Membrane Science, 428 (2013) 403-409.

[11] M. Ben-Sasson, X. Lu, E. Bar-Zeev, K.R. Zodrow, S. Nejati, G. Qi, E.P. Giannelis, M. Elimelech, In situ formation of silver nanoparticles on thin-film composite reverse osmosis membranes for biofouling mitigation, Water research, 62 (2014) 260-270.

[12] J. Yin, Y. Yang, Z. Hu, B. Deng, Attachment of silver nanoparticles (AgNPs) onto thin-film composite (TFC) membranes through covalent bonding to reduce membrane biofouling, Journal of Membrane Science, 441 (2013) 73-82.

[13] M. Ben-Sasson, K.R. Zodrow, Q. Genggeng, Y. Kang, E.P. Giannelis, M. Elimelech, Surface Functionalization of Thin-Film Composite Membranes with Copper Nanoparticles for Antimicrobial Surface Properties, Environmental science & technology, 48 (2014) 384-393.

[14] S. Kang, M.S. Mauter, M. Elimelech, Microbial Cytotoxicity of Carbon-Based Nanomaterials: Implications for River Water and Wastewater Effluent, Environmental Science & Technology, 43 (2009) 2648-2653.

[15] A. Tiraferri, C.D. Vecitis, M. Elimelech, Covalent Binding of Single-Walled Carbon Nanotubes to Polyamide Membranes for Antimicrobial Surface Properties, ACS Applied Materials & Interfaces, 3 (2011) 2869-2877.

[16] F. Perreault, M.E. Tousley, M. Elimelech, Thin-Film Composite Polyamide Membranes Functionalized with Biocidal Graphene Oxide Nanosheets, Environmental Science & Technology Letters, 1 (2014) 71-76.

[17] H.S. Lee, S.J. Im, J.H. Kim, H.J. Kim, J.P. Kim, B.R. Min, Polyamide thin-film nanofiltration membranes containing TiO2 nanoparticles, Desalination, 219 (2008) 48-56.

[18] M. Hu, B. Mi, Enabling Graphene Oxide Nanosheets as Water Separation Membranes, Environmental science & technology, 47 (2013) 3715-3723.

[19] K.S. Novoselov, A.K. Geim, S.V. Morozov, D. Jiang, Y. Zhang, S.V. Dubonos, I.V. Grigorieva, A.A. Firsov, Electric Field Effect in Atomically Thin Carbon Films, Science, 306 (2004) 666-669.

[20] D.R. Dreyer, S. Park, C.W. Bielawski, R.S. Ruoff, The chemistry of graphene oxide, Chemical Society Reviews, 39 (2010) 228-240.

[21] F. Perreault, A. Fonseca de Faria, M. Elimelech, Environmental applications of graphene-based nanomaterials, Chemical Society Reviews, 44 (2015) 5861-5896.

[22] Y. Zhu, S. Murali, W. Cai, X. Li, J.W. Suk, J.R. Potts, R.S. Ruoff, Graphene and Graphene Oxide: Synthesis, Properties, and Applications, Advanced Materials, 22 (2010) 3906-3924.

[23] A.F. de Faria, D.S.T. Martinez, S.M.M. Meira, A.C.M. de Moraes, A. Brandelli, A.G.S. Filho, O.L. Alves, Anti-adhesion and antibacterial activity of silver nanoparticles supported on graphene oxide sheets, Colloids and Surfaces B: Biointerfaces, 113 (2014) 115-124.

[24] E.S. Orth, J.E.S. Fonsaca, S.H. Domingues, H. Mehl, M.M. Oliveira, A.J.G. Zarbin, Targeted thiolation of graphene oxide and its utilization as precursor for graphene/silver nanoparticles composites, Carbon, 61 (2013) 543-550.

[25] A.F. de Faria, F. Perreault, E. Shaulsky, L.H. Arias Chavez, M. Elimelech, Antimicrobial Electrospun Biopolymer Nanofiber Mats Functionalized with Graphene Oxide–Silver Nanocomposites, ACS applied materials & interfaces, 7 (2015) 12751-12759.

[26] W.S. Hummers, R.E. Offeman, Preparation of Graphitic Oxide, Journal of the American Chemical Society, 80 (1958) 1339-1339.

[27] V.C. Tung, M.J. Allen, Y. Yang, R.B. Kaner, High-throughput solution processing of large-scale graphene, Nat Nano, 4 (2009) 25-29.

[28] F. Perreault, A.F. de Faria, S. Nejati, M. Elimelech, Antimicrobial Properties of Graphene Oxide Nanosheets: Why Size Matters, ACS Nano, 9 (2015) 7226-7236.

[29] Y. Yin, Z.-Y. Li, Z. Zhong, B. Gates, Y. Xia, S. Venkateswaran, Synthesis and characterization of stable aqueous dispersions of silver nanoparticles through the Tollens process, Journal of Materials Chemistry, 12 (2002) 522-527.

[30] A. Tiraferri, N.Y. Yip, A.P. Straub, S. Romero-Vargas Castrillon, M. Elimelech, A method for the simultaneous determination of transport and structural parameters of forward osmosis membranes, Journal of Membrane Science, 444 (2013) 523-538.

[31] M. Xie, E. Bar-Zeev, S.M. Hashmi, L.D. Nghiem, M. Elimelech, Role of Reverse Divalent Cation Diffusion in Forward Osmosis Biofouling, Environmental Science & Technology, 49 (2015) 13222-13229.

[32] S. Liu, M. Hu, T.H. Zeng, R. Wu, R. Jiang, J. Wei, L. Wang, J. Kong, Y. Chen, Lateral Dimension-Dependent Antibacterial Activity of Graphene Oxide Sheets, Langmuir, 28 (2012) 12364-12372.

[33] A. Panáček, M. Kolář, R. Večeřová, R. Prucek, J. Soukupová, V. Kryštof, P. Hamal, R. Zbořil, L. Kvítek, Antifungal activity of silver nanoparticles against Candida spp, Biomaterials, 30 (2009) 6333-6340.

[34] L. Liu, J. Liu, Y. Wang, X. Yan, D.D. Sun, Facile synthesis of monodispersed silver nanoparticles on graphene oxide sheets with enhanced antibacterial activity, New Journal of Chemistry, 35 (2011) 1418-1423.

[35] J. Tang, Q. Chen, L. Xu, S. Zhang, L. Feng, L. Cheng, H. Xu, Z. Liu, R. Peng, Graphene Oxide–Silver Nanocomposite As a Highly Effective Antibacterial Agent with Species-Specific Mechanisms, ACS Applied Materials & Interfaces, 5 (2013) 3867-3874.

[36] J. Li, C.-y. Liu, Ag/Graphene Heterostructures: Synthesis, Characterization and Optical Properties, European Journal of Inorganic Chemistry, 2010 (2010) 1244-1248.

[37] C. Li, X. Wang, F. Chen, C. Zhang, X. Zhi, K. Wang, D. Cui, The antifungal activity of graphene oxide–silver nanocomposites, Biomaterials, 34 (2013) 3882-3890.

[38] T.S. Sreeprasad, S.M. Maliyekkal, K.P. Lisha, T. Pradeep, Reduced graphene oxide–metal/metal oxide composites: Facile synthesis and application in water purification, Journal of Hazardous Materials, 186 (2011) 921-931.

[39] H.J. Kim, A.E. Fouda, K. Jonasson, In situ study on kinetic behavior during asymmetric membrane formation via phase inversion process using Raman spectroscopy, Journal of Applied Polymer Science, 75 (2000) 135-141.

[40] L.M. Malard, M.A. Pimenta, G. Dresselhaus, M.S. Dresselhaus, Raman spectroscopy in graphene, Physics Reports, 473 (2009) 51-87.

[41] F. Perreault, H. Jaramillo, M. Xie, M. Ude, L.D. Nghiem, M. Elimelech, Biofouling Mitigation in Forward Osmosis Using Graphene Oxide Functionalized Thin-Film Composite Membranes, Environmental Science & Technology, 50 (2016) 5840-5848.

[42] W. Choi, J. Choi, J. Bang, J.-H. Lee, Layer-by-Layer Assembly of Graphene Oxide Nanosheets on Polyamide Membranes for Durable Reverse-Osmosis Applications, ACS Applied Materials & Interfaces, 5 (2013) 12510-12519.

[43] M.S. Mauter, Y. Wang, K.C. Okemgbo, C.O. Osuji, E.P. Giannelis, M. Elimelech, Antifouling Ultrafiltration Membranes via Post-Fabrication Grafting of Biocidal Nanomaterials, ACS Applied Materials & Interfaces, 3 (2011) 2861-2868.

[44] M. Rai, A. Yadav, A. Gade, Silver nanoparticles as a new generation of antimicrobials, Biotechnology Advances, 27 (2009) 76-83.

[45] I. Sondi, B. Salopek-Sondi, Silver nanoparticles as antimicrobial agent: a case study on E. coli as a model for Gram-negative bacteria, Journal of Colloid and Interface Science, 275 (2004) 177-182.

Thin-film composite forward osmosis membranes functionalized with graphene oxide–silver nanocomposites for biofouling control

Supplementary Data

Andreia F. Faria[1], Caihong Liu[1,2], Ming Xie[1,3], Francois Perreault[1,4], Long D. Nghiem[5], Jun Ma[2], and Menachem Elimelech [1*]

[1]*Department of Chemical and Environmental Engineering, Yale University, New Haven, Connecticut 06520-8286, USA*

[2] *State Key Laboratory of Urban Water Resource and Environment,* Harbin Institute of Technology, *Harbin 150090, China*

[3]*Institute for Sustainability and Innovation, College of Engineering and Science, Victoria University, PO Box 14428, Melbourne, Victoria 8001, Australia*

[4]*School of Sustainable Engineering and the Built Environment, Arizona State University, Tempe, AZ, 85287-3005.*

[5] *Water Infrastructure Laboratory, School of Civil, Mining and Environmental Engineering, University of Wollongong, Wollongong, NSW 2522, Australia*

* Corresponding author: Menachem Elimelech, Email: menachem.elimelech@yale.edu, Phone: (203) 432-2789
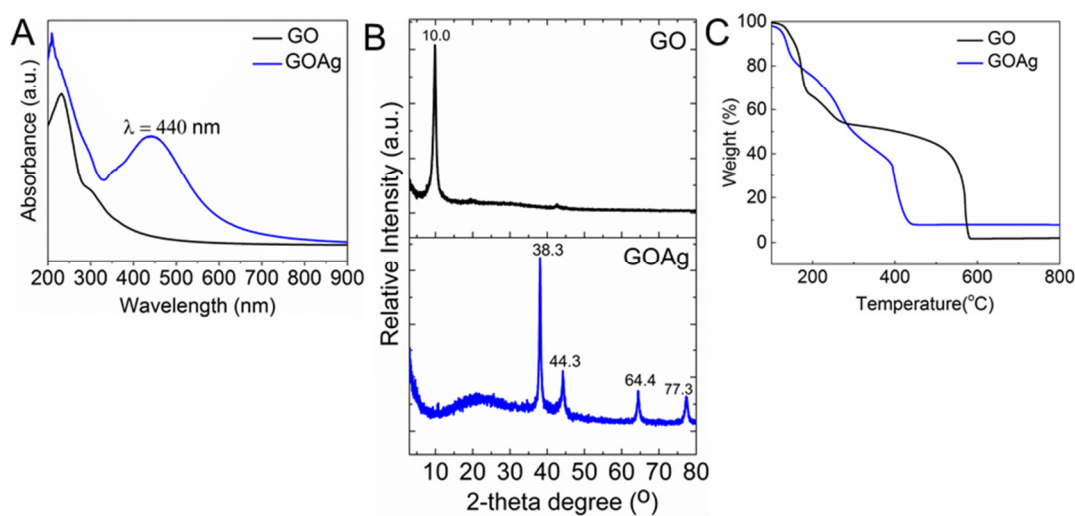
Figure S1: (A) UV-Vis spectra of GO and GOAg suspensions (100 µg mL^{-1}). The presence of plasmonic band at 440 nm suggests the formation of GOAg nanocomposite. (B) XRD spectra of GO and GOAg. The 2θ peaks at 38.3, 44.3, 64.4, and 77.3 are related to the crystalline planes of silver nanoparticles. (C) Thermogravimetric curves (TGA) of GO and GOAg shows their loss of weight at high temperatures. The residues above 600°C can be associated with the content of silver in the GOAg sample.
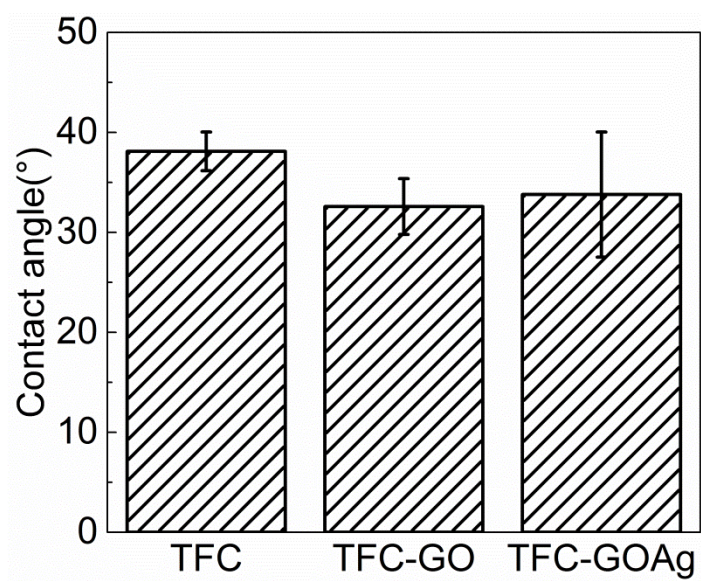
Figure S2: Water contact angle for unmodified TFC, TFC-GO, and TFC-GOAg membranes.

Table S1: Estimation of water and salt permeability coefficients of TFC, TFC-GO, and TFC-GOAg membranes by the FO four-step characterization method [1]. The final water permeability coefficient *A*, salt permeability coefficient *B*, and structural parameter *S* presented in the manuscript were determined from three sets of independent measurements for each membrane.

Membrane	Step	J_w (Lm^{-2}h^{-1})	J_s (mmolm^{-2}h^{-1})	J_w/J_s (Lmmol^{-1})	R^2-J_w	R^2-J_s
TFC	i	12.42	81.2	0.19		
	ii	17.35	104.1	0.197	0.988	0.985
	iii	20.47	128.6	0.209		
	iv	25.72	155.18	0.219		
TFC-GO	i	13.66	78.8	0.173		
	ii	18.03	104.8	0.172	0.997	0.998
	iii	23.06	129.8	0.178		
	iv	27.68	155.14	0.178		
TFC-GOAg	i	12.42	81.2	0.153		
	ii	17.35	104.1	0.167	0.989	0.994
	iii	20.47	128.6	0.159		
	iv	25.72	155.18	0.166		

Reference:

[1] A. Tiraferri, N.Y. Yip, A.P. Straub, S. Romero-Vargas Castrillon, M. Elimelech, A method for the simultaneous determination of transport and structural parameters of forward osmosis membranes, Journal of Membrane Science, 444 (2013) 523-538.